Mon. Not. R. Astron. Soc. **000**, 1–12 (2004) Printed 21 January 2005 (MN LATEX style file v2.2)

High Galactic latitude polarized emission at 1.4 GHz and implications for cosmic microwave background observations

E. Carretti[1]⋆, G. Bernardi[1], R.J. Sault[2], S. Cortiglioni[1] and S. Poppi[3]
[1] *CNR–IASF Bologna, Via Gobetti 101, Bologna, I-40129, Italy*
[2] *CSIRO–ATNF, P.O. Box 76, Epping, NSW 1710, Australia*
[3] *CNR–IRA Bologna, Via Gobetti 101, Bologna, I-40129, Italy*

Accepted xx xx xx. Received yy yy yy; in original form zz zz zz

ABSTRACT
We analyse the polarized emission at 1.4 GHz in a $3^\circ \times 3^\circ$ area at high Galactic latitude ($b \sim -40^\circ$). The region, centred in ($\alpha = 5^{\rm h}$, $\delta = -49^\circ$), was observed with the Australia Telescope Compact Array radio-interferometer, whose 3–30 arcmin angular sensitivity range allows the study of scales appropriate for Cosmic Microwave Background Polarization (CMBP) investigations. The angular behavior of the diffuse emission is analysed through the E- and B-mode angular power spectra. These follow a power law $C_\ell^X \propto \ell^{\beta_X}$ with slopes $\beta_E = -1.97 \pm 0.08$ and $\beta_B = -1.98 \pm 0.07$. The emission is found to be about a factor 25 fainter than in Galactic plane regions. The comparison of the power spectra with other surveys indicates that this area is intermediate between strong and negligible Faraday rotation effects. A similar conclusion can be reached by analysing both the frequency and Galactic latitude behaviors of the diffuse Galactic emission of the 408-1411 MHz Leiden survey data. We present an analysis of the Faraday rotation effects on the polarized power spectra, and find that the observed power spectra can be enhanced by a transfer of power from large to small angular scales. The extrapolation of the spectra to 32 and 90 GHz of the CMB window suggests that Galactic synchrotron emission leaves the CMBP E-mode uncontaminated at 32 GHz. The level of the contamination at 90 GHz is expected to be more than 4 orders of magnitude below the CMBP spectrum. Extrapolating to the relevant angular scales, this region also appears adequate for investigation of the CMBP B-modes for models with tensor-to-scalar fluctuation power ratio $T/S > 0.01$. We also identify polarized point sources in the field, providing a 9 object list which is complete down to the polarized flux limit of $S^p_{\rm lim} = 2$ mJy.

Key words: cosmology: cosmic microwave background – polarization – radio continuum: ISM – diffuse radiation – radiation mechanisms: non-thermal.

1 INTRODUCTION

Polarized Galactic synchrotron emission is one of the most important foregrounds in measuring the Cosmic Microwave Background Polarization (CMBP) up to about 100 GHz. Above that frequency dust emission becomes the dominant contaminant. Moreover, as the fractional polarization of the synchrotron emission can be 30% and as CMBP is just few percent of the CMB anisotropy, the degree of contamination is expected to be worse than in temperature anisotropy measurements.

The study of this foreground is thus crucial for CMBP experiments. It will allow an estimate of the contamination level, and will aid developing cleaning procedures to remove its contribution from the cosmic signal (e.g. see Tegmark et al. 2000 and references therein).

The CMBP emission peaks on sub-degree angular scales in the 5–30 arcmin range (e.g. see Zaldarriaga, Spergel & Seljak 1997). Consequently, observations of CMBP can be carried on in small sky patches that are large enough to allow good statistics (5°–10° wide) but, at the same time, small enough to minimize environmental systematics, e.g. spillover from ground emission. The latter could swamp the detection of the faint (few μK) cosmic signal. Small regions, moreover, have the additional advantage of allowing a part of the sky low in synchrotron contamination to be selected.

The synchrotron emission can be best observed at low frequency, where it dominates other diffuse components (dust, free-free, and CMBP itself) and where the signal strength allows easier detection by radiotelescopes. To date,

⋆ E-mail: carretti@bo.iasf.cnr.it

analysis of the Galactic synchrotron has been performed by several surveys at frequencies up to 2.7 GHz. These have been mainly concentrated on the Galactic plane, where the signal is greater. The Southern Galactic Plane Survey (SGPS, Gaensler et al. 2001) and the Canadian Galactic Plane Survey (CGPS, Taylor et al. 2003) are interferometric surveys whose main goal is to map almost all the Galactic plane at 1.4 GHz down to a 1 arcmin resolution. These surveys provide deep insight into many effects typical of Galactic polarized emission (e.g., polarization horizons, Faraday screens). However, because of their interferometric origin, these surveys are sensitive to angular scales no larger than the 30 arcmin of the telescope primary beam.

The largest angular scales are instead covered by a single dish project: the Effelsberg 1.4 GHz Medium Galactic Latitude Survey (EMLS, Uyanıker et al. 1999 and Reich et al. 2004). This covers the Galactic plane up to medium latitudes ($|b| < 20^\circ$). The approximately 10 arcmin resolution allows EMLS to overlap the scales accessible by the two previous interferometric surveys, and their combination will provide full information on the Galactic plane down to 1 arcmin.

The Galactic plane has been also surveyed at higher frequency by Duncan et al. (1997) and Duncan et al. (1999). They covered about a half of the plane at 2.4 and 2.7 GHz, respectively, with the latitude coverage extends to $|b| < 5^\circ$.

The mid Galactic latitudes has been partially surveyed at 350 MHz by the Westerbork survey (Haverkorn, Katgert & de Bruyn 2003), which mapped the polarized emission at longitudes $l \sim 140^\circ$–170° and up to $b = 30^\circ$. Because of their lower frequency, these data are likely to be more affected by Faraday rotation effects.

The analysis of the Galactic plane region has provided the first information on the angular behavior of the Galactic synchrotron radiation (see Bruscoli et al. 2002 and references therein). However, the optimal locations for observations of the CMBP are at high latitudes, where the emission is low. High latitude regions are not as well studied, although more recent surveys are starting to fill this gap, at least at 1.4 GHz.

Sparse observations at all Galactic latitudes were made in 1960s and 1970s (e.g. Baker & Wilkinson 1974; Brouw & Spoelstra 1976, and references therein). Among them, the observations presented by Brouw & Spoelstra (1976) covered all Galactic latitudes at 5 frequencies between 408 and 1411 MHz. For decades these have represented the largest data set of polarized measurements out of the Galactic plane. Although undersampled and not suitable for a full investigation of the synchrotron characteristics (especially when dealing with the angular behavior) some analyses of the angular power spectra have been carried out in the best sampled portions (Bruscoli et al. 2002). Moreover, as we will see in this work, this data-set can provide useful information on the frequency behavior of the large angular scale structure.

The whole of the Northern and Southern sky are being mapped by Wolleben et al. (2004) and Testori, Reich & Reich (2004), respectively, at 1.4 GHz. These surveys are very precious, since they will provide the first all-sky map of the polarized emission at 1.4 GHz down to the degree scale. They are sensitive to the large angular scale structure of the polarized emission in interesting (for CMBP purposes) low emission regions. However, their angular resolution (larger than 30 arcmin) and sensitivity (about 15 mK) do not allow the analysis of the faint areas required by sub-degree CMBP experiments, which require better resolution (finer than 30 arcmin) and sensitivity (rms signal about 10 mK, see Bernardi et al. 2003).

All of the aforementioned surveys are at low frequencies, where the Faraday rotation effects can still play a significant role. In fact, Faraday rotation can introduce a randomization of polarization angles which transfers power from large to small angular scales by modifying the polarized emission pattern. Although this transfer of power has been claimed to explain some results at frequencies up to 1.4 GHz (e.g Tucci et al. 2002), it has not been quantitatively studied. A detailed study is needed to evaluate its effect before we can safely extrapolate up to the mm-wave cosmological window.

The patch of sky near $\alpha = 5^{\rm h}$ and $\delta = -50^\circ$ has been identified as an interesting area for CMBP investigations: it is at high Galactic latitude ($b \sim -40^\circ$) and, from an analysis of the Rhodes/HartRAO 2326-MHz radio continuum survey (Jonas, Baart & Nicolson 1998), it is expected to have a synchrotron emission at the low level required for CMBP studies (Bernardi 2004; Carretti et al. 2002). In fact, this region was chosen for the total intensity observation by the BOOMERanG experiment and has been selected as target for BaR-SPOrt (Cortiglioni et al. 2003) and BOOMERanG-B2K (Masi et al. 2002).

This patch has been observed in polarization at 1.4 GHz to a sensitivity to allow detection of the polarized synchrotron emission (Bernardi et al. 2003). This represents the first detection of this emission at high Galactic latitude at this frequency and in the angular scale range useful for CMBP analyses (5–30 arcmin).

These observations, along with an initial analysis of the implications for CMBP studies, have been presented by Bernardi et al. (2003). In the present paper we perform a more detailed analysis of the polarized emission in this area and reach firmer conclusions regarding CMBP implications.

We quantatively analyse the effects of the polarization angle randomization introduced by Faraday screens, finding that a power transfer from large to small angular scales occurs. This results both in a steepening of the (angular) spectral index and an enhancement of the observed emission on the angular scales our observations are sensitive to (i.e. 3–30 arcmin). This implies that our measurements represent an upper limit of the intrinsic polarized emission.

We present the angular power spectra of the E- and B-modes. Comparison of these with other surveys suggests that the observed patch is an intermediate state between significant and negligible Faraday rotation effects.

Finally, we extrapolate the spectra up to the frequency range of CMB measurements (30–90 GHz). This suggests that the Galactic synchrotron emission is low enough in this area that it should not be an issue for both the E-mode (from 30 GHz) and the fainter B-mode (provided a tensor-to-scalar power ratio $T/S > 0.01$).

The paper is organized as follows. In Section 2 we present a quick summary of the observations. In Sections 3 and 4 we analyse the point sources detected in the field and the Rotation Measure (RM). Section 5 discusses the power transfer from large to small angular scales as a result of randomization of polarization angles. It considers how this

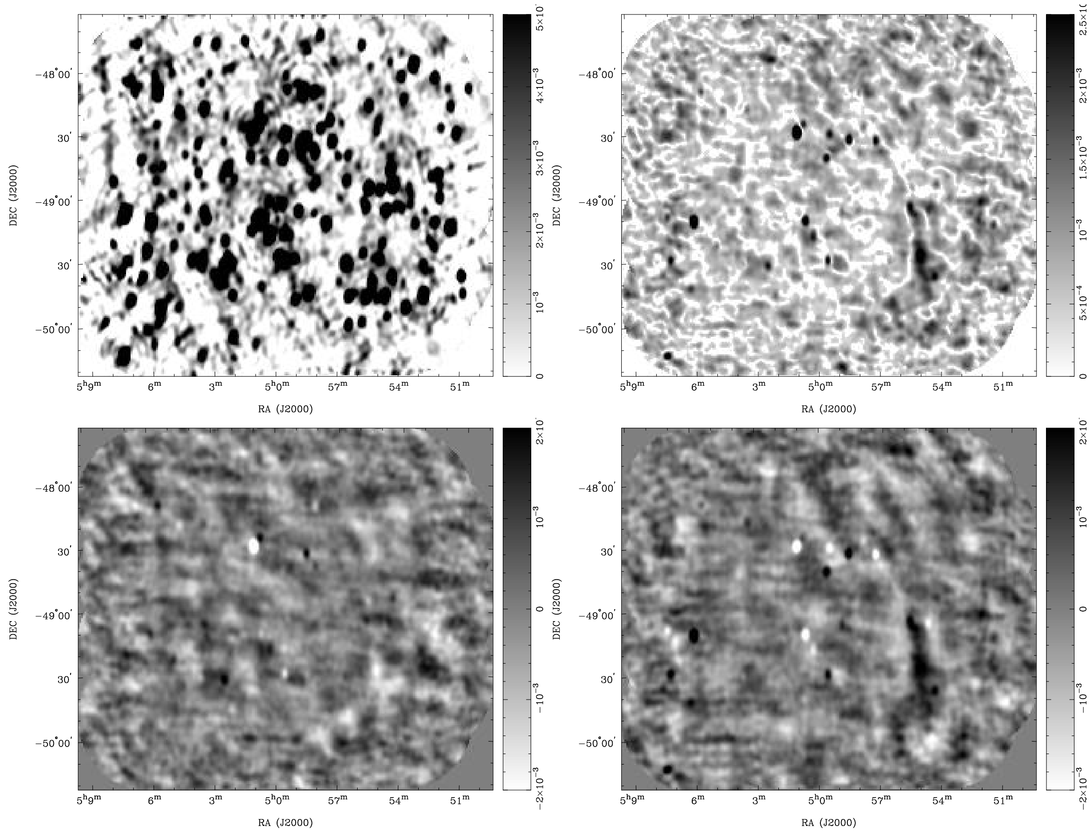

Figure 1. From top-left, clockwise: I, I^p, U and Q maps at 1.4 GHz of the $3° \times 3°$ area centred on $\alpha = 5^{\rm h}$, $\delta = -49°$. Values are Jy beam^{-1}. Point sources have not been subtracted. (See Bernardi et al. 2003 for polarized maps cleaned from point sources.)

changes the polarized power spectrum. The E- and B-mode power spectra of the synchrotron emission in the patch will be presented in Section 6 together with an analysis of the role of Faraday rotation effects. The implications for CMBP investigations are discussed in Section 7. Summary and conclusions are finally presented in Section 8.

2 OBSERVATIONS

The region centred on ($\alpha = 5^{\rm h}$, $\delta = -49°$) has been observed at 1.4 GHz by Bernardi et al. (2003) using the Australia Telescope Compact Array (ATCA, Frater, Brooks & Whiteoak 1992), an East-West synthesis interferometer situated near Narrabri (NSW, Australia), operated by CSIRO-ATNF.

The observation was performed as a 49 pointing mosaic covering a $3° \times 3°$ region. The array configuration used was the so-called EW214 including spacing from 30 m to 214 m. This provides sensitivity on angular scales ranging from ~ 30 arcmin down to the resolution of ~ 3.4 arcmin. The system provides the four Stokes parameters I, Q, U, V. Details of the observations are listed in Table 1 and presented in Bernardi et al. (2003).

The maps of the Stokes parameters I, Q and U, along with the polarized intensity $I^p = \sqrt{Q^2 + U^2}$, are shown in Figure 1. Differing from Bernardi et al. (2003), here no subtraction of polarized point sources has been performed.

The polarized emission I^p is *patchy* in nature, and distributed over the whole field. An exception is a bright feature in the South-West corner of the area: it is more filamental, being about 1° long. The Stokes I image does not show any particular diffuse structure at the same coordinates, although the point source contamination makes the comparison hard. As in other high resolution observations (e.g. Wieringa et al. 1993; Gaensler et al. 2001), a *Faraday screen* is likely acting along the line of sight. This acts as a small scale modulation of a relatively uniform background, generating the apparent filamental structure on small angular scales.

The mean polarized emission $P_{\rm rms} = \sqrt{\langle Q^2 \rangle + \langle U^2 \rangle} = 11.6$ mK found by Bernardi et al. (2003) is well above the beam sensitivity ($S/N \sim 3.5$) allowing an analysis of the synchrotron emission features in the area.

Table 1. Main characteristics of the 1.4 GHz observations.

Central Frequency	1380 MHz
Effective Bandwidth	205 MHz
Array Configuration	EW214
Angular Sensitivity Range	3.4–30 arcmin
Location (J2000)	$\alpha = 5^{\rm h}$, $\delta = -49°$
Area Size	$3° \times 3°$
Observation Period	June 2002
Effective Observing Time	~ 70 h
Sensitivity (flux)	0.18 mJy beam^{-1}
Sensitivity (temperature)	3.2 mK beam^{-1}

Table 2. Position, total intensity (I) and polarized intensity (I^p) of the 9 sources detected in the field. The rms-error is the same for both the two intensities and corresponds to the beam-sensitivity (0.18 mJy beam^{-1}). Polarization angle (ϕ) and polarization degree ($\Pi = I^p/I$) are also reported. Counterparts were located in radio catalogues. Where no radio-counterpart was found, the closest optical object found in both the APM and 2-MASX surveys is listed (see text for details). The last column provides the distance from the counterpart.

source	RA J2000	DEC J2000	I [mJy]	I^p [mJy]	ϕ	Π	counterpart	distance [arcmin]
1	$5^h01^m01^s.4$	$-48°31'03''.0$	164.10	10.72	$15.4° \pm 0.5°$	6.5%	PMN J0501-4831	0.5
2	$5^h05^m58^s.8$	$-49°11'43''.0$	98.52	6.63	$21.5° \pm 0.8°$	6.7%	2MASX J05055521-4910485	1.1
3	$4^h58^m34^s.5$	$-48°34'40''.2$	130.20	3.71	$43.8° \pm 1.4°$	2.9%	APMUKS(BJ) B045704.24-483820.7	1.8
4	$5^h00^m38^s.2$	$-49°12'29''.5$	139.70	3.40	$43.6° \pm 1.5°$	2.4%	PMN J0500-4912	0.2
5	$4^h59^m37^s.8$	$-48°43'13''.6$	38.21	2.78	$41.3° \pm 1.9°$	7.3%	APMUKS(BJ) B045822.87-484738	0.9
6	$5^h07^m08^s.8$	$-49°29'32''.0$	20.73	2.75	$-27.5° \pm 1.9°$	13.3%	2MASX J05070829-4929268	0.1
7	$4^h57^m17^s.7$	$-48°34'58''.5$	23.93	2.32	$42° \pm 3°$	9.7%	APMUKS(BJ) B045558.02-483812.5	1.3
8	$5^h07^m24^s.5$	$-50°13'14''.4$	123.70	2.18	$40° \pm 2°$	1.8%	PKS 0506-502	0.2
9	$4^h59^m29^s.7$	$-48°31'56''.9$	55.48	2.01	$44° \pm 3°$	3.6%	PMN J0500-4912	0.3

3 POINT SOURCES

Even though the field has been selected to minimize their contamination, a few point sources are present in the polarized intensity map (Figure 1). To identify them, we fit the maxima/minima in Q and U maps with a 2D-Gaussian beam and a constant value using MIRIAD's task IMFIT (Sault, Teuben & Wright 1995). The constant value is adopted to account for the background emission. We keep only those sources where the resultant Full Width at Half Maximum (FWHM) is compatible with the synthesized beam. Sources providing larger FWHM are instead discarded, the fit being not able to separate the background emission.

For the detections, we retain only those point sources where the emission is 3 times the rms signal of the diffuse component ($S/P_{\rm rms} > 3$). This gives good confidence that we avoid confusion between point sources and statistical fluctuations of the diffuse background, while ensuring a solid detection above the instrumental noise ($S/N > 10$). Moreover, this criterium allows us to provide a complete list down to the polarized flux of $S^p_{\rm lim} = 2.0$ mJy.

Given to these criteria, we find 9 sources: these are listed in Table 2.

We have attempted to identify the sources in published catalogues such as the Parkes-MIT-NRAO (PMN, Griffith & Wright 1993) survey. PMN was performed at 4.85 GHz, so that, assuming a mean spectral index $\alpha = 0.7$, its $S_{4.85} =$ 42 mJy flux-limit corresponds to about $S_{1.4} \sim 100$ mJy at 1.4 GHz. Accepting this, we would expect sources 1, 2, 3, 4 and 8 to be present in the PMN catalogue. However only sources 1, 4 and 8 were found: we are not able to find any identification for sources 2 and 3. It is worth noting that their fluxes are near the catalogue limit: a steeper spectrum would result in PMN failing to detect them. Conversely, source 9 has a PMN counterpart, even if the measured 1.4 GHz flux is about a half of the limit extrapolated from 4.85 GHz.

When a PMN counterpart could not be found, we looked for the closest object present in the optical/IR catalogues APM (Maddox et al. 1990) and 2-MASX (Huchra et al. 2003), provided it lies within a FWHM of the detected radio source. Possible counterparts have been found for all the missing objects. These are listed in Table 2. It is worth noting that all of these sources are classified as normal galaxies.

Given the limited number of sources, no general properties can be extracted. We simply note that only one source exceeds the 10% polarization.

4 ROTATION MEASURE

The magnetic field parallel to the line of sight ($B_\parallel$) changes the polarization angle by Faraday rotation. The variation $\Delta\phi = \phi - \phi_0$ with respect to the intrinsic polarization angle ϕ_0 is given by the formula

$$\Delta\phi = RM\ \lambda^2, \qquad (1)$$

where λ is the wavelength of the radiation and RM is the Rotation Measure. The latter is defined by the integral along the line of sight

$$RM = 0.81 \int B_\parallel(l)\ n_e(l)\ dl \qquad (2)$$

which depends on $B_\parallel(l)$ and the free-electron density $n_e(l)$ in the Interstellar Medium (ISM) at various distances l from the observer.

Beside changing in the polarization vector direction and, in turn, in the naive estimate of the magnetic field orientation, Faraday rotation can induce both depolarization effects and Faraday screen modulations. These can significantly modify the angular power distribution and pattern of the polarized emission. RM estimates in the patch of sky being consider are thus important in understanding the significance of these effects.

Because the ATCA correlator produces a number of frequency channels across the observed bandwidth, we are able to determine values of RM from our data set. Faraday rotation has been evaluated by grouping the 26 useful channels of our observations in four sub-bands to form four maps of Q, U and V at the different frequencies of 1316, 1368, 1404 and 1454 MHz. For each frequency, the Stokes V map sets the noise level for the corresponding Q and U maps. Using MIRIAD's task IMPOL, we have obtained maps of polarized

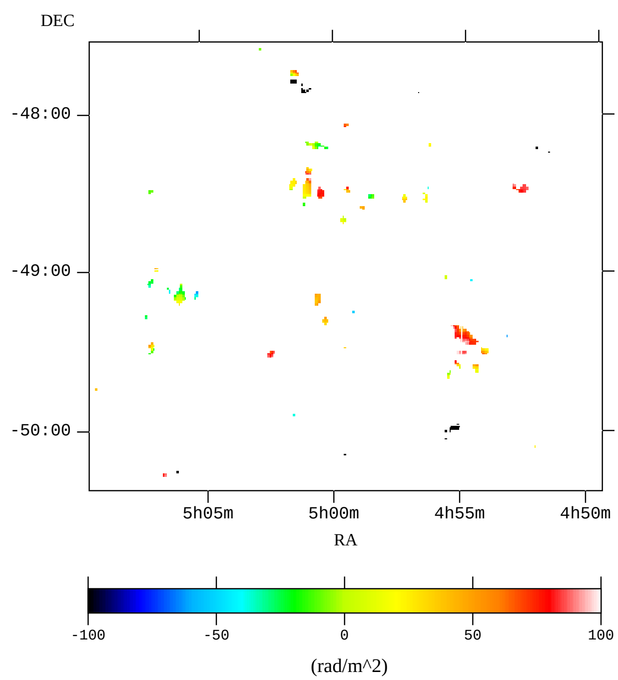

Figure 2. Map of *RM*s measured in the patch.

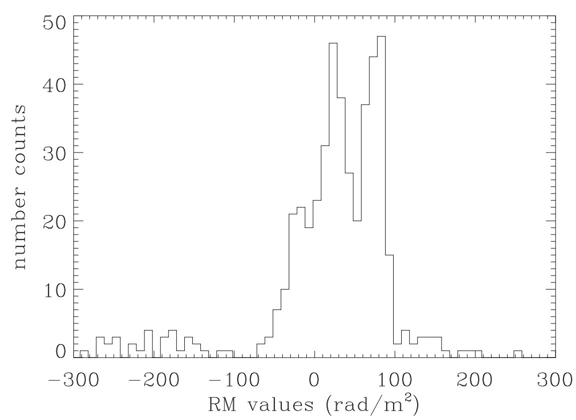

Figure 3. Distributions of the measured *RM*s.

intensity and polarization angle at each frequency. *RM* values are then determined using MIRIAD's task IMRM, that fits a *RM* map from polarization angles at the different frequencies. This task also tries to solve the $N\pi$ ambiguity in the *RM* determination. Pixels with an error in polarization angle greater than 20° are discarded.

The *RM* values that were successful determined by this process are shown in Figure 2. The coverage of the measurements in the patch is sparse, and so they cannot be considered to be fully representative of the area. However, they are scattered over all the field and thus give a useful indication of the broader trend. The distribution, shown in Figure 3, presents two peaks: the first near 20 rad m^{-2} and a second near 80 rad m^{-2}. Apart from a small number of points, the measurements of the second peak relate to the filament structure. This is thus characterized by *RM* values larger than typical of this patch. This might be expected if the filament is caused by a Faraday screen. The other measurements of *RM* lie near the first peak. Thus 20 rad m^{-2} can be considered a typical value of the *RM* of the successful pixels.

This result is in good agreement with other estimates of *RM* in this region. The all-sky catalogue of rotation measures for extragalactic sources by Broten, MacLeod & Vallée (1988) contains four sources within 5° from the centre of the area. These have *RM* values of 13, 28, 34 and 53 rad m^{-2}. The rotation measure maps of Han et al. (1997) and Johnston-Hollitt, Hollitt & Ekers (2004) are indicative of large-scale *RM* values. In our area, they suggest values of approximately 20–30 rad m^{-2} (see Han 2004 for a review).

Given these various estimates of *RM*, we can consider $RM = 50$ rad m^{-2} as a reasonable upper limit for the typical rotation measure within the patch. As in Bernardi et al. (2003), this value in combination with the total bandwidth of the ATCA observations implies a depolarization factor of $D \sim 92\%$. This has a marginal impact on our main goal of estimating the level of polarized synchrotron emission in the area.

5 POWER TRANSFER FROM LARGE TO SMALL SCALES

As noted by several authors (e.g. see Wieringa et al. 1993 and Gaensler et al. 2001), Faraday screens can introduce a small scale modulation of a relatively uniform background. If a complex Faraday screen is interposed between the observer and a uniform polarized emission, the *RM* pattern of the screen will cause modulation of polarization angle, resulting in variable patterns of Q and U. This causes transferring power from large to small angular scales in polarization maps, and generates *false* small scale structures.

Figure 4 demonstrates this point using a simple model: the intrinsic emission is uniform, while the observed one is sinusoidal. This is caused by a *RM* which varies linearly with angle. A result of the process is that angular power that had corresponded to the large scale structure has been transferred down to the modulation scale.

Overall the effect randomizes the polarized emission larger than a particular angular scale.

Although this effect has been invoked as a qualitative explanation of structures observed, we are not aware of a quantitative analysis having been performed.

Here we simulate some realistic examples to estimate importance and main features of the effect. First, we generate Q and U maps starting from E- and B-mode angular power spectra which we assume have power law behavior

$$\begin{aligned} C^E &\propto \ell^{\beta_E}, \\ C^B &\propto \ell^{\beta_B}, \end{aligned} \qquad (3)$$

with the spectral indeces which can be

$$\beta_X = 0.0,\ -1.5,\ -3.0, \qquad X = E, B. \qquad (4)$$

These have been selected in a range wide enough to cover all of the cases observed to date for the polarized Galactic synchrotron emission and are centred on the most common measured values ($\beta_X = -1.6$, e.g. see Bruscoli et al. 2002; Giardino et al. 2002).

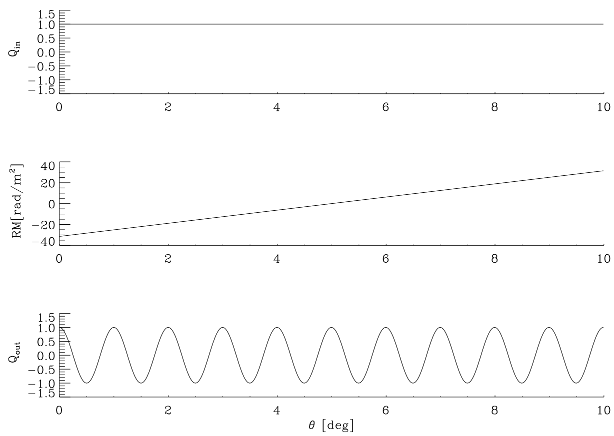

Figure 4. A simple model showing how a variable *RM* pattern can transform uniform emission to one modulated on smaller angular scales. The top panel shows a background with uniform emission on a 10° box-size (emission of Stokes Q only is assumed, i.e. $\phi_0 = 0°$). The mid panel shows *RM* varying linearly. The *observed* Q is shown in the bottom panel, assuming a 300 MHz frequency. The *observed* emission is modulated on 1° scale, smaller than the intrinsic emission.

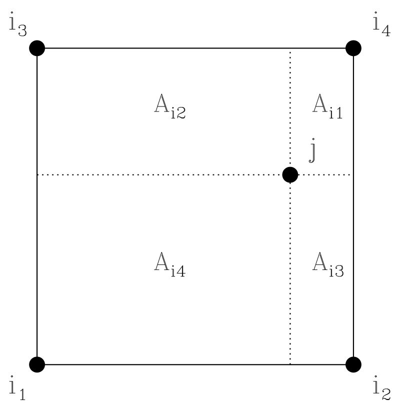

Figure 5. CIC scheme for regularly gridded data. The four grid points i_1, i_2, i_3 and i_4 are the nearest to the pixel j where the quantities sampled on the grid points have to be interpolated. A_{i_k} with $k = 1, 4$ are the opposite sub-cells used in the weighted mean.

We use the `synfast` procedure of the HEALPix package (Górski, Hivon & Wandelt 1999) to generate the maps given the power spectra. We adopt an angular resolution of about 2 arcmin (HEALPix's parameter $N_{\rm side} = 2048$) to match the angular resolution of the observed maps (about 3.4 arcmin). Finally, 20° × 20° square maps are extracted.

The area we observed shows a polarization angle pattern uniform at least up to 10–15 arcmin scale (see Bernardi et al. 2003). In this simulation, we assume that the polarization angles are totally random above 15 arcmin angular scale size. This is done by placing a 15 arcmin × 15 arcmin grid on the simulated map, and then assigning a random polarization rotation angle to each grid point.

To associate a random angle with each pixel of the map, the random angles of the nearest grid points are linearly interpolated to the pixel position by using a Cloud-in-Cell (CIC) scheme (Hockney & Eastwood 1981). In order to explain the procedure, let us define θ_i as the random angle associated to the $i^{\rm th}$ point of the grid and j the $j^{\rm th}$ pixel of the map where the angles have to be interpolated. Referring to Figure 5, the CIC method consists first in finding the 4 grid points i_1–i_4 which are the nearest to the pixel j and which define the Cell where j itself is located. The linear interpolation is performed assigning to j a weighted mean of the values sampled on these 4 points: the pixel j divides the Cell in four sub-cells and the weight of a grid point is proportional to the area of the sub-cell opposite to the point itself:

$$\theta_j = \frac{\sum_{k=1}^{4} A_{i_k}\, \theta_{i_k}}{\sum_{k=1}^{4} A_{i_k}}, \tag{5}$$

where θ_j is the quantity to be estimated at the pixel j, i_k with $k = 1, 4$ are the four nearest grid points and A_{i_k} are the areas of the corresponding sub-cells.

We have adopted this linear interpolation scheme to avoid the discontinuities that a simple Nearest Grid Point (NGP) scheme would produce in the polarization angle map.

Figure 6 shows the power spectra C^E before and after the randomization procedure. The results for C^B are similar. For the case $\beta_E = 0.0$, there is no change in the power at any scale. This is expected as this case corresponds to a totally random pattern of Q and U ($C_\ell = constant$ is the case of pure white noise): adding further randomization does not change the statistics of the data.

In the other two cases the randomization reduces the power on the largest scales, while increasing it on the smallest ones. In particular, on the scales that the interferometer is sensitive to (3–30 arcmin), the power is greater or equal to that of the input maps.

Randomization of the large-scale polarization angle thus does transfer power from large to small angular scales. On the small scales, the angular power detected is an enhancement. Consequently what we measure is an upper limit to the intrinsic fluctuation.

The angular scale which marks the transition from reduction to enhancement depends on the power law index. However, at least for the range explored here, it is larger than the scale size of the randomization. Because our map has a randomization scale of at least 15 arcmin, the power detected in the 3–30 arcmin range is enhanced or at least not reduced. Consequently, in terms of power spectra, our measurements represents an upper limit of the real emission.

From Figure 6, we can consider the slope of the power spectrum: this power spectrum is steeper in those ℓ-ranges where the power is enhanced. Indeed, apart from a transition range centred at the randomization scale, the modified spectra follows a power law but with a steeper slope. This is in agreement with the results of Tucci et al. (2002). They found spectra at 1.4 GHz that were steeper than at 2.4 GHz, where Faraday effects are weaker.

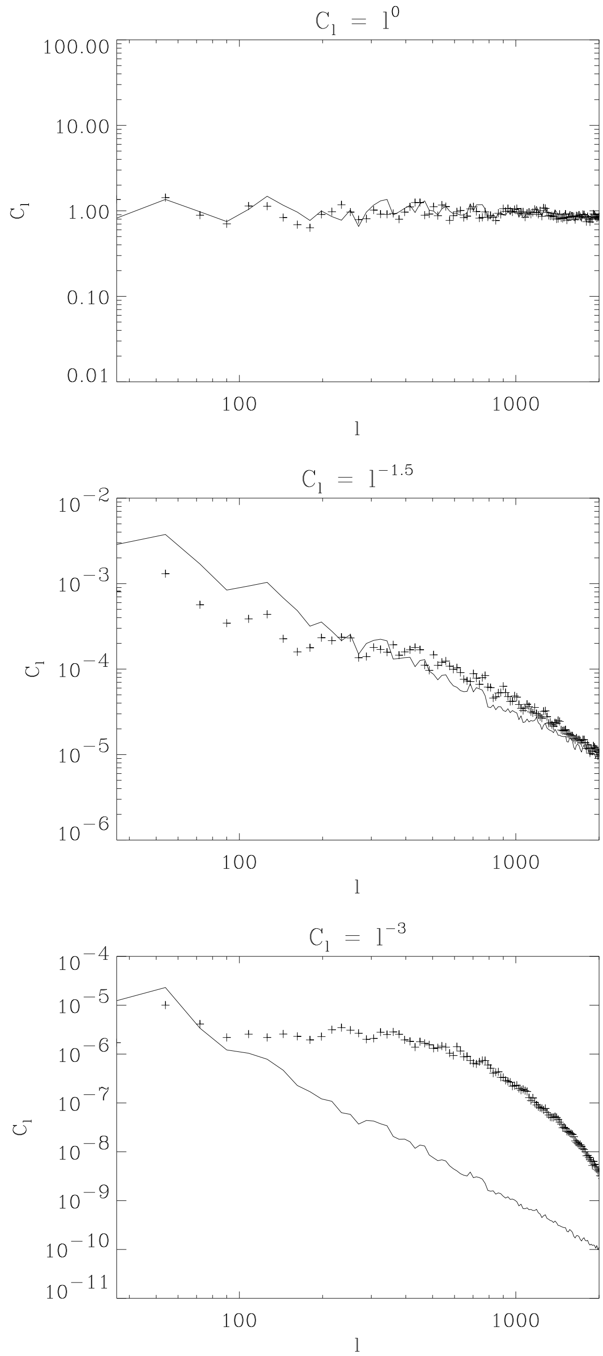

Figure 6. C^E power spectra for the three models described in the text (β_E = 0.0, -1.5, -3.0) before (solid lines) and after (crosses) the application of the polarization angle randomization procedure.

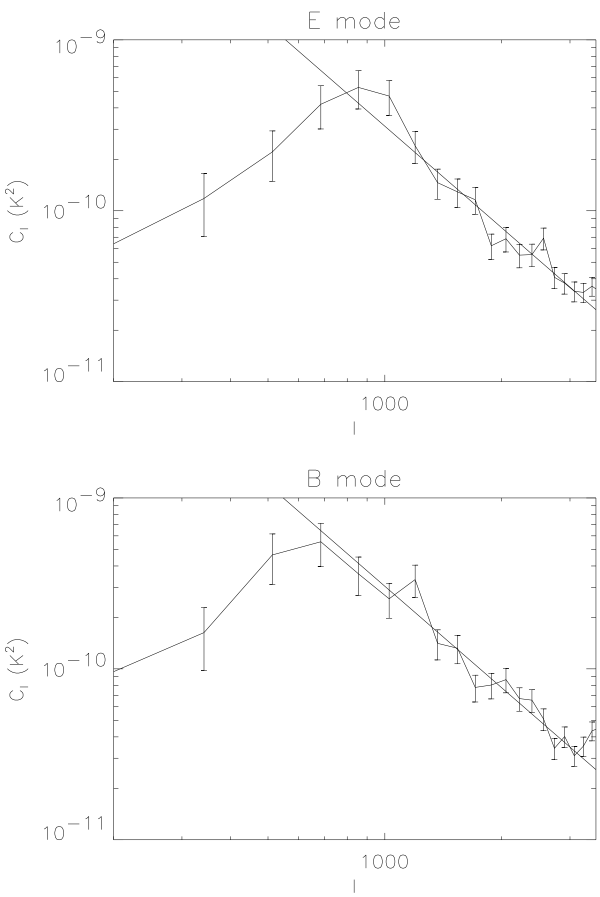

Figure 7. E- (top) and B-mode (bottom) angular power spectra of the polarized emission at 1.4 GHz in the observed patch.

6 POWER SPECTRUM ANALYSIS

E- and B-modes, combinations of the tensorial 2-spin quantities $Q \pm j\,U$, completely describe the polarized emission and have the useful characteristic of being scalar (e.g. see Zaldarriaga & Seljak 1997; Zaldarriaga 1998). Thus, they allow us to describe how the polarized signal is distributed across angular scales by using simple scalar spherical harmonics.

We prefer these descriptors instead of the scalar spectra of Q and U because the latter depend on the orientation of the reference frame. Additionally, E- and B-spectra are the quantities predicted by cosmological models. Their use for Galactic work allows a direct comparison between the Galactic and cosmological signals and the evaluation of the contamination of the latter by the former.

We have computed the E- and B-mode spectra by using the Fourier technique of Seljak (1997). The results are shown in Figure 7. Both power spectra are well approximated by a power law on scales smaller than about 15 arcmin (multipoles $\ell > 800$). On larger scales, there is a turn-over and power becomes negligible for $\ell <$ 300–400. This corresponds to about the 30 arcmin antenna primary beam size. This turn-over is a result of the spatial filtering of an interferometer. The ATCA has little sensitivity on scales larger than about the FWHM of the primary beam, has somewhat improved sensitivity between about FWHM and FWHM/2, and shows full sensitivity on scales smaller than about FWHM/2.

The power law behavior covers the 3.4–15 arcmin range of full sensitivity of the instrument. Table 3 gives the results when we fit the functional form

$$C_\ell^X = C_{2000}^X \left(\frac{\ell}{2000}\right)^{\beta_X}, \qquad X = E, B, \tag{6}$$

in the ℓ–range of 800–2800.

It is interesting to compare the amplitude and spectral

Table 3. Best fit parameters of the angular power spectra of our 1.4 GHz data.

Spectrum	C^X_{2000} [10^{-11} K^2]	β_X
C^E_ℓ	8.0 ± 0.2	−1.97 ± 0.08
C^B_ℓ	8.0 ± 0.2	−1.98 ± 0.07

Table 4. Slopes β_X of angular power spectra of the Galactic synchrotron polarized emission. The table also reports the sky area the slope has been computed for and the observation frequency. SGPS–2.4 refers to the slope computed from the 2.4 GHz survey (Duncan et al. 1997) in the area covered by the SGPS Test Region. The last column reports the references where the slopes have been measured.

Area	β_X	frequency	Ref.
This area	~ -2.0	1.4 GHz	this work
SGPS	~ -2.8	1.4 GHz	Tucci et al. (2002)
SGPS-2.4	~ -1.7	2.4 GHz	Tucci et al. (2002)
Galactic plane	~ -1.6	2.4–2.7 GHz	Bruscoli et al. (2002)

index with information from other Galactic surveys. First, let us consider the SGPS Test Region (Gaensler et al. 2001). This covers a similar area (about $4^\circ \times 6^\circ$). Like the current study, the SGPS Test Region survey is an interferometric observation at arcminute resolution and carried out at the same 1.4 GHz frequency. However, its region of interest is located on the Galactic plane.

The first significant difference is in the amplitude: SGPS has a $C^X_{2000} \sim 5 \times 10^{-8}$ K^2 (Tucci et al. 2002), corresponding to a signal about 25 times stronger than in the patch of the current study. This is expected, as the observed patch is at high Galactic latitudes. Furthermore this is consistent with the result of Bernardi et al. (2003), which found that the mean signal of this patch is about 10 times smaller than the background emission in areas close to the Galactic plane of the 1.4 GHz EMLS survey (Uyanıker et al. 1999). However it is worth noting that the difference is not as large as the case with total intensity: in total intensity the differences between Galactic plane and high Galactic latitudes emissions can be much larger – for instance, see the full-sky surveys at 408 MHz (Haslam et al. 1982) and 1.4 GHz (Reich & Reich 1986; Reich, Testori & Reich 2001).

Another area of significant difference is the slopes of the power spectra (Table 4). The power laws in the observed patch have $\beta_X \sim -2.0$, which is considerably flatter than $\beta^{\rm SGPS}_X \sim -2.8$ for the SGPS (Tucci et al. 2002). However it is close to the $\beta^{\rm SGPS-2.4}_X \sim -1.7$ found at 2.4 GHz in the region covered by the SGPS, but using the data of Duncan et al. (1997) (Tucci et al. 2002). The latter agrees with the mean value $\bar\beta^{2.4-2.7}_X \sim -1.6 \pm 0.2$ measured at 2.4–2.7 GHz over a large portion of the Galactic Plane (Bruscoli et al. 2002).

The large difference between $\beta^{\rm SGPS-2.4}_X$, $\bar\beta^{2.4-2.7}_X$ and $\beta^{\rm SGPS}_X$ was first addressed by Tucci et al. (2002), who explained the steepening of the SGPS through a Faraday-rotation induced transfer of power from large to small scales. Section 5 provides a quantitative approach to this effect: Faraday screens can introduce randomization in the polarization angle, which actually transfer power from large to small angular scales and, thus, increases the power and the slope on scales smaller than the randomization scale size.

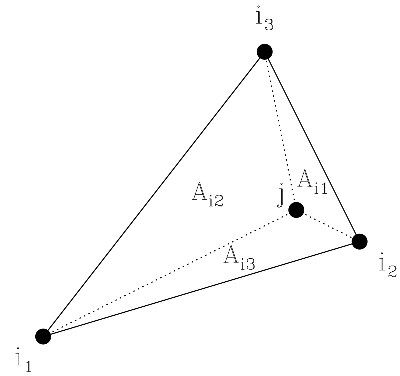

Figure 8. As for Figure 5 but using the modified CIC scheme dealing with irregularly sampled data (see text for details).

Faraday rotation has a square dependence on the wavelength and the effects at 2.4 GHz are expected to be less significant than at 1.4 GHz. The flatter slope at 2.4 GHz can be interpreted as a reduction of the effects of Faraday rotation. The slopes most probably are near the intrinsic value.

Moreover, in spite of a large variation of *RM*s across the Galactic plane, the slopes measured at 2.4–2.7 GHz have a small dispersion ($\Delta\beta^{2.4-2.7}_X = 0.2$), indicating a good stability around the mean value. This further supports the idea that the 2.4–2.7 GHz slopes are slightly modified by Faraday effects and are near the intrinsic values.

Our results are lie between the two previous values. In fact, pulsar and extragalactic source measurements show that the *RM* becomes less significant at high Galactic latitudes: starting from the typical value $|RM| \sim 200$ rad m^{-2} at the Galactic Plane (e.g. Gaensler et al. 2001), through 20–30 rad m^{-2} at mid Galactic latitudes (Han et al. 1997; Johnston-Hollitt et al. 2004) and down to 10–20 rad m^{-2} in the North Galactic Pole (NGP) (e.g. see Sun & Han 2004). Hence we would expect to see less impact of Faraday rotation in the observed patch than in the SGPS. We conclude that our observed patch is in an intermediate domain between significant and negligible Faraday rotation effects.

We have analysed the data of Brouw & Spoelstra (1976), which has led us to a similar conclusion. In more detail, the data of Brouw & Spoelstra (1976) give polarization observations of about a half of the sky at five frequencies: 408, 465, 610, 820, 1411 MHz. Having the desirable characteristics of covering all the Northern Galactic latitudes and a wide range in frequency, these data allow us to explore behavior in both frequency and latitude. An issue with this data-set is that it is sparsely sampled and arranged on irregular grids. While the lowest frequency case is tolerable (the best sampled areas have about 2° sampling versus a FWHM = 2.3°) the situation is worst at 1411 MHz, where FWHM = 0.6°. Nevertheless, regridding and smoothing on angular scales larger than the sampling distance allow the analysis of the characteristic of the emission at least for the large scale structure.

To account for irregular sampling, we regrid the data on regular HEALPix maps via linear interpolation, using a variant of the CIC scheme. The standard CIC deals with data sampled on a regular grid, as described in Section 5. On the other hand, here the data are sampled on irregular grids. Let (Q_i, U_i) be the $i^{\rm th}$ sample of the grid and j the $j^{\rm th}$ pixel of the map to be interpolated. Referring to Figure 8, we generalize the CIC scheme finding the 3 grid points (i_1, i_2, i_3) which define the smallest triangle containing j. Connecting j to i_1, i_2 and i_3, three triangular sub-cells can be identified. Similarly to Eq. (5), the linear interpolation is performed assigning to j an average of the values sampled on these 3 grid points weighted for the area of the opposite sub-cell:

$$X_j = \frac{\sum_{k=1}^{3} A_{i_k}\, X_{i_k}}{\sum_{k=1}^{3} A_{i_k}}, \qquad X = Q, U, \tag{7}$$

where X_j is the quantity to be estimated at the pixel j.

The deformations of the 2-sphere space can generate depolarization due to the projection of Q and U onto the local reference frame of parallels and meridians if a simple mean of the data is performed. Close to the NGP, this will be a particular issue. Following Bruscoli et al. (2002), to avoid these projection effects, we perform a parallel transport of the polarization vectors (Q_{i_k}, U_{i_k}) onto the interpolation point j before averaging the data.

To account for the irregular sampling distance, the interpolated data are smoothed with a Gaussian filter of 4° FWHM, leading to maps able to describe the large scale distribution of the polarized emission.

The resultant maps at the 5 frequencies are shown in Figure 9. A feature is clearly visible in the Fan region at Galactic longitude $l \sim 150°$ at all frequencies. This region is close to the area where the line of sight is nearly perpendicular to the local Galactic magnetic field. Hence, there is only a small parallel magnetic field component, and so small Faraday rotation effects. Consequently the presence of a large non-depolarized region is not surprising, even at the lowest frequency.

For the current study, the area of most interest is at very high Galactic latitudes. The North Galactic Spur, while depolarized at 408 MHz, becomes evident with increasing frequency. Moreover, this structure is apparent at the highest latitudes first and propagates toward lower ones as frequency increases: while at 610 MHz the large scale polarized structure is evident only close to the NGP, at 820 MHz it is present down to $b \sim 60°$ and reaches $b \sim 40°$ at 1411 MHz.

The polarization angle maps exhibit similar behavior. While complex at low frequency, the polarization angle pattern becomes more regular in the NGP region at the highest frequencies. At 610 MHz, the region of ordered behavior is limited to the very high latitude areas. Order expands to lower latitudes with increasing frequency, reaching $b \sim 40°$–$50°$ at 1411 MHz.

It is easy to interpret this in light of the previous discussion. The randomization of the polarization angles due to Faraday rotation, transferring the power from large to small scales, destroys the polarized emission on the largest scales at the lowest frequencies. At higher frequencies, the effects of Faraday rotation decrease, leading to the re-appearing of the large scale structures. This starts in the areas with smaller *RM*. Considering the *RM* behavior with Galactic latitudes, we expect that this would start at the very high latitudes and expand to the mid latitudes with increasing frequency, producing larger *ordered* regions showing the intrinsic structure.

This analysis of the Brouw & Spoelstra (1976) data supports that our patch, given the observing parameters (at 1.4 GHz and $|b| \sim 40°$), is in an intermediate state between strong and negligible influence of the Faraday rotation.

7 IMPLICATIONS FOR CMBP

The E- and B-mode spectra of Section 6 are the first measurements for a high Galactic latitude patch at 1.4 GHz on sub-degree scales (i.e. scales on which CMBP has most of the power).

Other spectra out of the Galactic plane ($b < 30°$) have been measured by Haverkorn et al. (2003), but at lower frequency (~ 350 MHz). Their results show slopes with a very large distribution, suggesting significant changes of Faraday rotation. However, a decrease in slope toward higher Galactic latitudes seems to exist, in agreement with the interpretation given here.

Our data are at a significantly higher frequency and, being less affected by Faraday rotation features, are to date the most suitable for extrapolation to the frequency range of CMB measurements.

Figure 10 shows the E-mode spectrum extrapolated up to the 32 and 90 GHz frequencies of the BaR-SPOrt experiment, assumed the synchrotron follows a power law

$$T_{\rm synch} \propto \nu^{\gamma} \tag{8}$$

with spectral index $\gamma = -3.1$, typical of the 1.4–23 GHz spectral range (Bernardi et al. 2004). These spectra include the correction for the square of the conversion factor

$$c = \left[\frac{2\,\sinh(x/2)}{x}\right]^2, \qquad x = h\nu/kT_{\rm cmb} \tag{9}$$

transforming antenna into thermodynamic temperature of CMB (ν is the frequency and $T_{\rm cmb} = 2.726$ K).

The presence of Faraday rotation effects makes the power in our images an upper limit to the intrinsic power on CMBP scales. Hence, apart from errors in the frequency spectral index, these extrapolations represent an upper limit of the contamination on the cosmic signal.

These results suggest that the synchrotron emission should only marginally contaminate the cosmological signal at 32 GHz, making this patch a good target for CMBP investigations. Even assuming an error of $\Delta\gamma = 0.2$ on the power law, the contamination would be only a factor 2 stronger, which does not change the conclusion.

The situation at 90 GHz is clearer still: the extrapolated spectrum is more than 4 orders of magnitude lower than the cosmic signal, leaving the CMBP practically uncontaminated by synchrotron pollution. Including the steepening of the synchrotron spectral index above 23 GHz observed by the WMAP team (Bennett et al. 2003b), the conclusion is very robust.

Such low emission of the Galactic synchtron makes this area promising even for the weak B-mode. Its emission has a peak near $\ell = 100$, whereas our data cover only the $\ell =$ 800–2800 range. To compare the emissions, in Figure 11 we

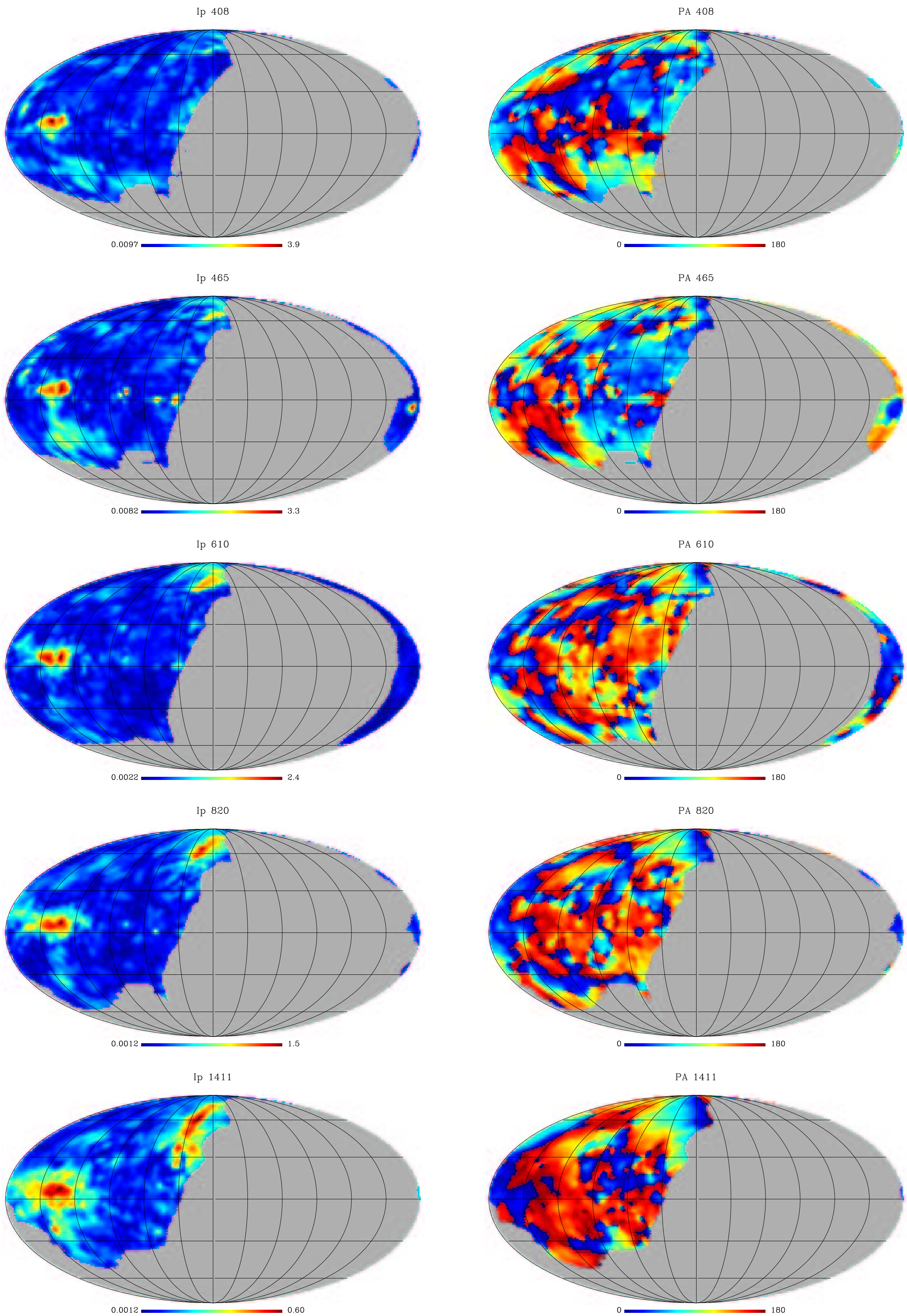

Figure 9. Polarized intensity I^p (left) and polarization angle maps (right) formed by interpolating the Brouw & Spoelstra (1976) data. The maps correspond to 408, 465, 610, 820, 1411 MHz (from top to bottom). The units are Kelvin and degrees, respectively. The maps, in Galactic coordinates centred on the Galactic centre, have been convolved with a 4° FWHM Gaussian filter.

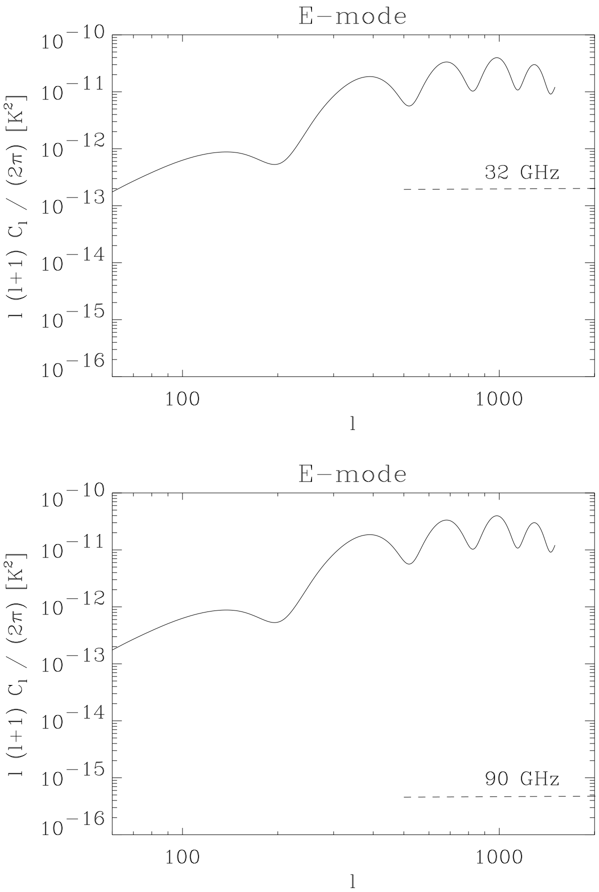

Figure 10. Fit of the E-mode spectrum measured for our data scaled up to 32 (top) and 90 GHz (bottom). The spectrum expected for CMBP with cosmological parameters as from WMAP results (Spergel et al. 2003) is also shown.

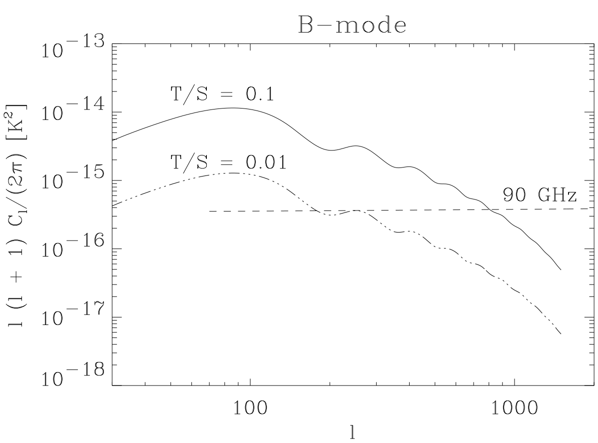

Figure 11. Fit of the B-mode spectrum measured for our data scaled up to 90 GHz. B-mode spectra expected for CMBP with tensor-to-scalar perturbations power ratios $T/S = 0.1$ and $T/S = 0.01$ are also shown. The other cosmological parameters are as from WMAP results (Spergel et al. 2003).

extrapolate the synchrotron spectrum down to $\ell = 100$ with the same slope of Table 3. In fact, since the slope we have measured at 1.4 GHz could be steeper than the intrinsic one, our estimate is somewhat conservative.

Figure 11 indicates that a model with tensor-to-scalar perturbation power ratio $T/S = 0.1$ should be well accessible in this area, the synchrotron contribution being a factor 30 fainter than the CMBP spectrum. This gap makes the result quite robust to errors in the extrapolation.

Even more interesting is that a model with $T/S = 0.01$ could be accessible in this part of the sky. At this low level it is likely that the leading contaminant will be the thermal dust, whose study requires measurements at higher frequencies (hundreds of GHz).

8 SUMMARY AND CONCLUSIONS

We have analysed the observation by Bernardi et al. (2003) of the polarized emission at 1.4 GHz in the high Galactic latitude area ($b \sim -40°$). This represents the first detection of the Galactic synchrotron polarized emission carried out in a low emission area at 1.4 GHz on this angular scale, giving us good data to estimate the contamination of the CMBP signal by the Galactic synchrotron radiation.

The contamination has been evaluated through the polarized angular power spectra C^E and C^B. These follows a power law behavior with spectral indeces $\beta_E = -1.97 \pm 0.08$ and $\beta_E = -1.98 \pm 0.07$. The emission level is about 25 times fainter than in Galactic plane regions.

Extrapolations to the CMB frequency window (30–100 GHz) gives encouraging results: the E-mode of CMBP is expected to be safely accessible already at 32 GHz, while at 90 GHz the margin is much larger ensuring clean measurements of CMBP. The low contamination level makes this patch a good candidate for the detection of the weaker B-mode: the tensorial signal appears accessible for models with $T/S > 0.01$.

The analysis of the Faraday rotation effects performed in this paper reinforces the robustness of our estimates. The low *RM* values measured in the patch (typically 20 rad m^{-2}) do not generate significant bandwidth depolarization. Additionally, we have carried out a quantitative analysis of the effects caused by the randomization of the polarization angles as a result of Faraday screens. We find an enhancement of the power on angular scales smaller than that of randomization, which ensures that the power we measure in the observed patch is an upper limit of the intrinsic emission – at least on the scales relevant for CMB purposes. Moreover, the analysis of the Faraday screen effects provides a second important result: a steepening of the power law index on angular scales smaller than that of randomization. The comparison between the slopes we have measured with those obtained by other surveys suggests the patch is in an intermediate state between significant and negligible Faraday rotation effects.

A similar conclusion is reached from an analysis of the data of Brouw & Spoelstra (1976). Depolarization effects are seen to decrease on the large scale polarized emission as the frequency increases from 408 MHz up to 1411 MHz. Starting from the NGP at the lowest frequencies, the large scale emission appears down to $b \sim 40°$ at 1411 MHz. This further supports the conclusion that the Galactic latitude of the observed patch is in an intermediate state between significant and negligible Faraday rotation effects at 1.4 GHz.

It appears that the patch is still affected by Faraday effects, but that it is very close to showing the intrinsic emission. Therefore, the estimates we have given here are conservative upper limits. Observations at higher frequency should allow measurements which are not affected by Faraday rotation.

ACKNOWLEDGMENTS

This work has been carried out as part of the SPOrt experiment, a programme funded by ASI (Italian Space Agency). G.B. acknowledge an ASI grant. We thanks T.A.Th. Spoelstra for providing us the Leiden survey data and M. Tucci for providing us his code for angular power spectrum computation. Part of this work is based on observations taken with the Australia Telescope Compact Array. The Australia Telescope Compact Array is part of the Australia Telescope, which is funded by the Commonwealth of Australia for operation as a National Facility managed by CSIRO. This research has made use of the NASA/IPAC Extragalactic Database (NED) which is operated by the Jet Propulsion Laboratory, California Institute of Technology, under contract with the National Aeronautics and Space Administration. We acknowledge the use of the HEALPix and CMBFAST packages.

REFERENCES

Baker J.R., Wilkinson A., 1974, MNRAS, 167, 581
Bennett C.L., et al., 2003, ApJS, 148, 97
Bernardi G., 2004, PhD thesis, Universitá di Bologna
Bernardi G., Carretti E., Cortiglioni S., Sault R.J., Kesteven M.J., Poppi S., 2003, ApJ, 594, L5
Bernardi G., Carretti E., Fabbri R., Sbarra C., Cortiglioni S., Poppi S., Jonas J.L., 2004, MNRAS, 351, 436
Broten N.W., MacLeod J.M., Vallée, 1988, Ap&SS, 141, 303
Brouw W.N., Spoelstra T.A.Th., 1976, A&AS, 26, 129
Bruscoli M., Tucci M., Natale V., Carretti E., Fabbri R., Sbarra C., Cortiglioni S., 2002, New Astron., 7, 171
Carretti E., et al., 2002, in De Petris M. & Gervasi M., eds, Experimental Cosmology at Millimeter Wavelengths, AIP Conf. Proc., 616, 140
Cortiglioni S., et al., 2003, in Warmbein B., ed., 16th ESA Symposium on European Rocket and Balloon Programmes and Related Research, ESA Proc. SP-530, p. 271
Duncan A.R., Haynes R.F., Jones K.L., Stewart R.T., 1997, MNRAS, 291, 279
Duncan A.R., Reich P., Reich W., Fürst E., 1999, A&A, 350, 447
Frater R.H., Brooks J.W., Whiteoak J.B., 1992, J. Electrical Electron. Eng. Australia, 12, 103
Gaensler B.M., Dickey J.M., McClure-Griffiths N.M., Green A.J., Wieringa M.H., Haynes R.F., 2001, ApJ, 549, 959
Giardino G., Banday A.J., Górski K.M., Bennett K., Jonas J.L., Tauber J., 2002, A&A, 387, 82
Górski K.M., Hivon E., Wandelt B.D., 1999, in Banday A.J., Sheth R.S. & da Costa L., eds, Proceedings of the MPA/ESO Cosmology Conference Evolution of Large-Scale Structure, Print Partners Ipskamp, NL, p. 37, astro-ph/9812350
Griffith M.R., Wright A.E., 1993, AJ, 105, 5
Han J.L., Manchester R.N., Berkhuijsen E.M., Beck R., 1997, A&A, 322, 98
Han J.L., 2004, in Uyanıker B., Reich W. & Wielebinski R., eds, The Magnetized Interstellar Medium, Copernicus GmbH, p. 3
Haslam C.G.T., Stoffel H., Salter C.J., Wilson W.E., 1982, A&AS, 47, 1
Haverkorn M., Katgert P., de Bruyn A.G., 2003, A&A, 403, 1045
Hockney R.W., Eastwood J.W., 1988, Computer Simulation Using Particles (New York: McGraw-Hill)
Huchra J., Jarrett T., Skrustikie M., Cutri R., Schneider S., Macri L., Steining R., Mader J., 2003, in IAUS Symposium 216, ASP Conf. Series, S-216, p. 172 The Magnetized Interstellar Medium, Copernicus GmbH, p. 13
Johnston-Hollitt M., Hollitt C.P., Ekers R.D., 2004, in Uyanıker B., Reich W. & Wielebinski R., eds, The Magnetized Interstellar Medium, Copernicus GmbH, p. 13
Jonas J.L., Baart E.E., Nicolson G.D., 1998, MNRAS, 297, 977
Maddox S.J., Sutherland W.J., Efstathiou G., Loveday J., 1990, MNRAS, 243, 692
Masi S., et al., 2002, in Cecchini S., Cortiglioni S., Sault R.J., Sbarra C., eds, Astrophysical Polarized Backgrounds, AIP Conf. Proc., 609, 122
Reich P., Reich W., 1986, A&AS, 63, 205
Reich P., Testori J.C., Reich W., 2001, A&A, 376, 861
Reich W., Fürst E., Reich P., Uyanıker B., Wielebinski R., Wolleben M., 2004, in Uyanıker B., Reich W. & Wielebinski R., eds, The Magnetized Interstellar Medium, Copernicus GmbH, p. 45
Sault R.J., Teuben P.J., Wright M.H.C., 1995, in Shaw R., Payne H.E., Hayes J.J.E., eds, ASP Conf. Series, 77, p. 433
Seljak U., 1997, ApJ, 482, 6
Spergel D.N., et al., 2003, ApJS, 148, 175
Sun X.H., Han J.L., 2004, in Uyanıker B., Reich W. & Wielebinski R., eds, The Magnetized Interstellar Medium, Copernicus GmbH, p. 25
Taylor A.R., et al., 2003, AJ, 125, 3145
Tegmark M., Eisenstein D.J., Hu W., de Oliveira-Costa A., 2000, ApJ, 530, 133
Testori J.C., Reich P., Reich W., 2004, in Uyanıker B., Reich W. & Wielebinski R., eds, The Magnetized Interstellar Medium, Copernicus GmbH, p. 57
Tucci M., Carretti E., Cecchini S., Nicastro L., Fabbri R., Gaensler B.M., Dickey J.M., McClure-Griffiths N.M., 2002, ApJ, 579, 607
Uyaniker B., Fürst E., Reich W., Reich P., Wielebinski R., 1999, A&AS, 138, 31
Wieringa M.H., de Bruyn A.G., Jansen D., Brouw W.N., Katgert P., 1993, A&A, 268, 215
Wolleben M., Landecker T.L., Reich W., Wielebinski R., 2004, in Uyanıker B., Reich W. & Wielebinski R., eds, The Magnetized Interstellar Medium, Copernicus GmbH, p. 51

Zaldarriaga M., PhD thesis, MIT
Zaldarriaga M., Seljak U., 1997, PRD, 55, 1822
Zaldarriaga M., Spergel D.N., Seljak U., 1997, ApJ, 488, 1

This paper has been typeset from a TEX/ LATEX file prepared by the author.